Meteoritics & Planetary Science 40, Nr 9/10, 1455–1471 (2005)
Abstract available online at http://meteoritics.org

Aorounga and Gweni Fada impact structures, Chad: Remote sensing, petrography, and geochemistry of target rocks

Christian KOEBERL[1*], Wolf Uwe REIMOLD[2], Gordon COOPER[2], Duncan COWAN[3], and Pierre M. VINCENT[4]

[1]Department of Geological Sciences, University of Vienna, Althanstrasse 14, A-1090 Vienna, Austria
[2]Impact Cratering Research Group, School of Geosciences, University of the Witwatersrand, Private Bag 3, P.O. Wits, Johannesburg, South Africa
[3]Cowan Geodata Services, 12 Edna Road, Dalkeith, Western Australia, Australia
[4]Département Sciences de la Terre, Université Blaise Pascal, F-63038 Clermont Ferrand, Cedex, France
[*]Corresponding author. E-mail: christian.koeberl@univie.ac.at

(Received 1 July 2005; revision accepted 23 July 2005)

Abstract–Shuttle Radar Topography Mission data was used to investigate the Aorounga and Gweni Fada impact structures in Chad as part of a new remote sensing study. We believe the results of various data treatments provide extensive new perspective on the macro-structural and topographic divisions for these two impact structures. Our remote sensing studies indicate revised diameters of Aorounga and Gweni Fada of 16 and 22 km, respectively. We selected samples from these two structures for their petrographic, geochemical, and Rb-Sr and Sm-Nd isotopic characteristics. In samples from both structures, evidence for shock metamorphism was found in the form of single or multiple sets of planar deformation features in quartz, which confirms the impact origin for both the Aorounga and Gweni Fada structures. The crystallographic orientations of PDFs indicate maximum shock levels of 20–30 GPa for samples from the central parts of both structures. The PDF orientations are characteristic for the orientations observed elsewhere in shocked sandstones, with the higher angles in the orientation histograms being fairly abundant. Geochemically, the rocks are typical upper-crustal sandstones.

INTRODUCTION

In 1994, only 15 confirmed impact structures were known in Africa (Koeberl 1994). Since then, three new African impact structures have been identified (Master and Reimold 2002): the 14 km in diameter Gweni Fada complex crater in Chad (see below), the 3.4 km in diameter Kgagodi basin structure in Botswana (Brandt et al. 2003), and the large (~80 km in diameter) Morokweng impact structure in South Africa (e.g., Reimold et al. 2002; Koeberl and Reimold 2003). In addition, the 220 m in diameter Sinamwenda structure in northern Zimbabwe has been proposed to be of impact origin (Master and Reimold 2000), but a confirmation of its impact origin is still outstanding.

Aorounga and Gweni Fada are the only impact craters known so far in Chad (Fig. 1). No detailed geological mapping has been performed yet at either of the two structures. The availability of samples is extremely limited, and a civil war raging in northern Chad in the 1990s has prevented more detailed field studies. In this paper, we contribute the results of a new remote sensing study and report, for the first time, petrographic and geochemical data for the only accessible rock suite from these two crater structures (samples collected by P. M. Vincent). A preliminary report of some of our data was published in an abstract form (Koeberl et al. 1998).

BACKGROUND ON THE GEOLOGY OF AOROUNGA AND GWENI FADA

To summarize the geology of the two craters, we rely on published geological information for Aorounga (Becq-Giraudon et al. 1992) and Gweni Fada (Vincent and Beauvilain 1996). The circular depression of Aorounga, which appears on some regional geographic maps (cf. Roland 1976; Becq-Giraudon et al. 1992), has a visible present-day diameter of ~13 km and is located in northern Chad about 110 km southeast of the Emi Koussi volcano in the Tibesti Massif (Fig. 2a). It is centered on 19°06′ N and 19°15′ E, and is situated in an area of the desert that is characterized by

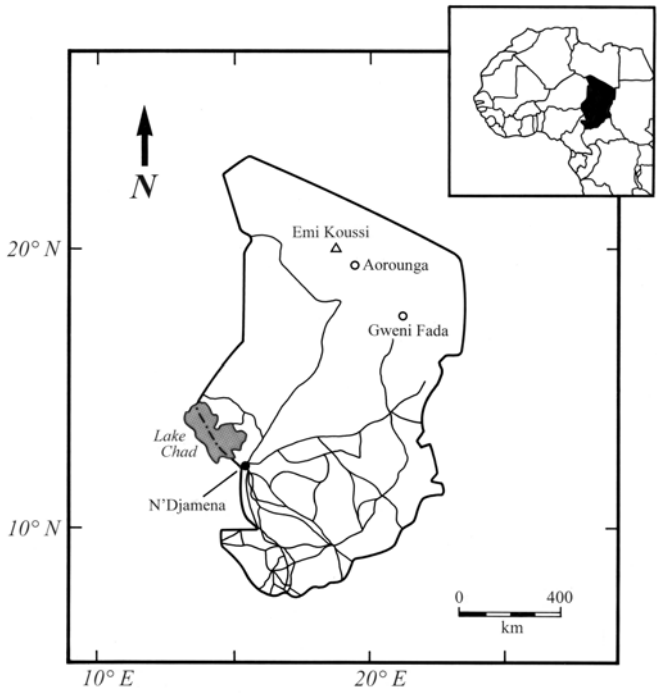

Fig. 1. Schematic map of central Africa showing the location of the two impact structures, Aorounga and Gweni Fada, in Chad (after Vincent and Beauvilain 1996).

strong wind erosion, which is expressed in the form of yardang-like sandstone ridges and depressions, as is clearly visible in shuttle imagery (Fig. 2a) and aerial photographs (Fig. 2b). Aorounga was originally studied in a photogeological investigation of Gemini, Apollo, Landsat, and aerial photographs by Roland (1976), who suggested an origin either as a granite diapir or an impact crater. However, this author favored the granite diapir hypothesis as the more likely explanation, but did not present any detailed arguments to support his idea. The structure was mentioned by Grieve et al. (1988) as a possible impact crater. About 15 years ago, a French expedition to the area succeeded in collecting a few samples from the structure and reported the first observation of shock deformation in the form of possible shatter cones and "shock-affected quartz" (Becq-Giraudon et al. 1992) (although the pictures given of these features in Becq-Giraudon et al. [1992] are not necessarily convincing).

The crater is formed in a fine-grained, well-sorted, slightly carbonate-bearing sandstone thought to be possibly of Upper Devonian age (Wacrenier et al. 1958). The structure is characterized by an outer and an inner ring (diameters of ~11 and 7 km, respectively), which both rise about 100 m above the mean level of the surrounding plain (Figs. 3a, b). The two rings are separated from each other by a depression of uniform width. A hill, or possible uplift structure, of ~1.5 km in diameter is located near the center of the central depression. The ring walls were described to consist of steeply outward dipping sandstone layers, with dips of 40–50° seen at the outer wall and 80° at the inner wall (Becq-Giraudon et al. 1992). Some breccia, described by Becq-Giraudon et al. (1992) as consisting of a coarse-grained siliceous matrix with fine-grained, beige clasts (cm- to dm-size) with fluidal texture, was apparently found on top of the inner rim wall. These same authors also described conical features that they interpreted to be shatter cones. Similar features are shown in Fig. 3c, but, due to the lack of laboratory studies on these samples, it is not entirely clear if they represent bona fide shatter cones or just wind erosion features, which can have a very similar appearance (e.g., Miller and Reimold 1986).

No reliable age dating exists for Aorounga. Based on the limited ^{14}C isotopic studies, Becq-Giraudon et al. (1992) estimated the age of the structure at only 12,000 to 3500 years, which appears to be incorrect, considering the seemingly strongly eroded nature of the structure (Figs. 2a–c). No melt-bearing samples that might provide a key for dating of the impact event have been identified among the limited sample suite available.

Bourles et al. (1995), who applied cosmogenic nuclides to in situ exposure dating, arrived at a minimum age of 0.5 Ma, and a range of 0.5–1 Ma was derived by Miallier et al. (1997) using thermoluminescence and electron spin resonance dating of quartz from Aorounga, again likely indicating a minimum age for this impact event. Thus, to conclude the available age information, it can only be said that, if the deformed target rocks were indeed of Upper Devonian age, then this provides the only real constraint on the upper age limit for the impact age currently available.

The second impact crater in Chad, the Gweni Fada structure, has been estimated to be ~14 km in diameter (Vincent and Beauvilain 1996). It is located about 320 km SE of Aorounga and 30 km NE of the Fada palm grove in the Ennedi district of northern Chad. A French team first noted it on Landsat images and aerial photography (Figs. 4a and b), and later visited it and reported the results of a preliminary petrographic study, which showed the presence of shock metamorphic effects in quartz grains from sandstones (Vincent and Beauvilain 1996).

The structure is centered at 17°25′ N and 21°45′ E. It appears asymmetric, being slightly wider in the NW-SE direction (cf. Fig. 6a), and deeply eroded. A broad depression (with a diameter of 12 km) forms a crescent around two thirds of the inner, seemingly structurally complex zone (see next section). The outer limit of the depression is pronounced, with steeply dipping (dip directions unknown) limestones marking the edge of this broad syncline. The depression is surrounded on the north side by an elevated outer ring of outward-dipping sandstones. On the south side, the external depression is absent, but tilted or folded sandstones are present (Vincent and Beauvilain 1996). The inner zone (with a diameter of about 10 km) consists of a rugged terrain with hills several hundred meters in elevation (Fig. 4b), which may represent the remnant of the central uplift, in which case the original diameter of the crater could have been significantly larger than 14 km (see below). Sandstones show irregular dips but

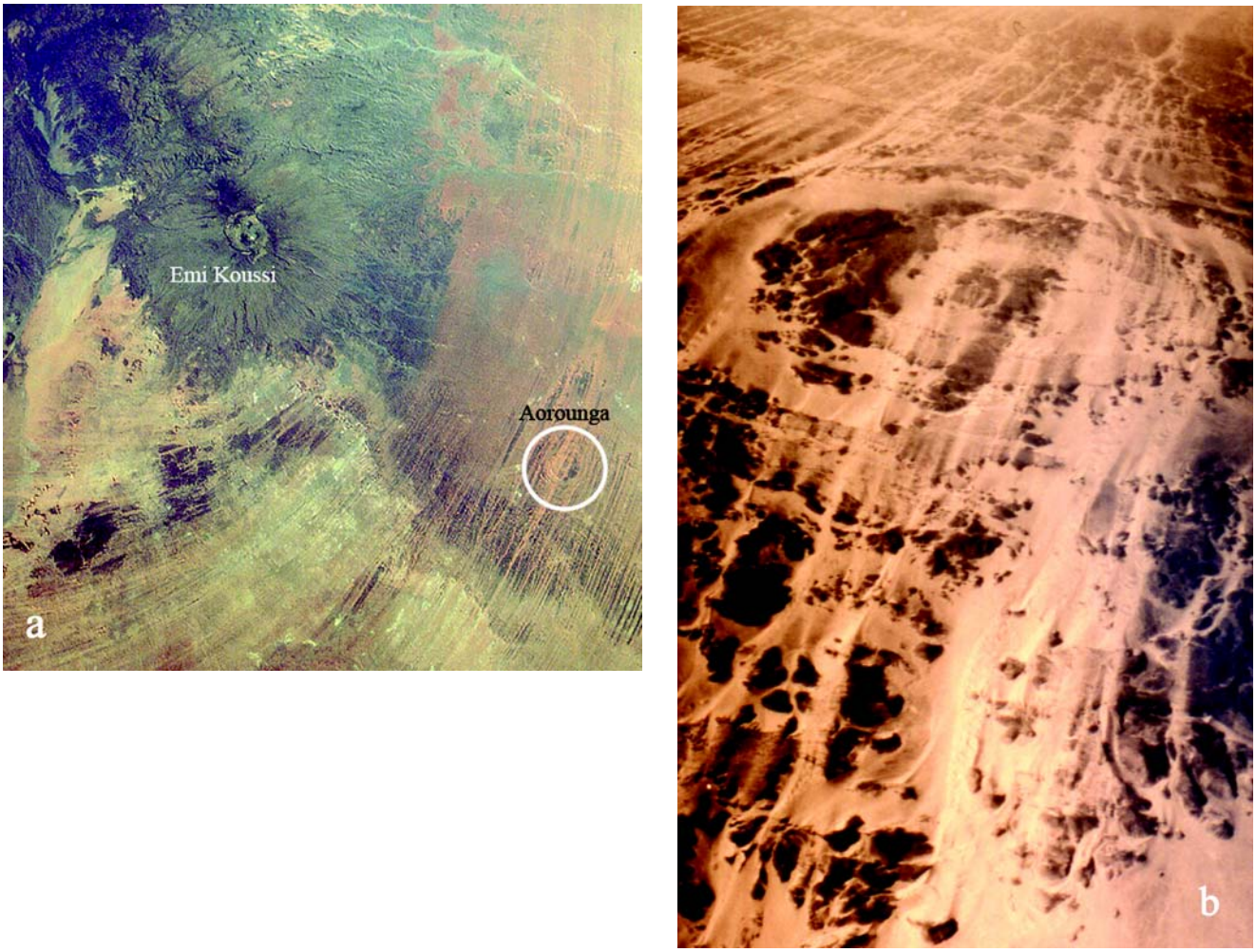

Fig. 2. a) Northern Chad, with the Emi Koussi volcano in the upper left part and the Aorounga impact structure in the lower right part of the image (space shuttle photograph STS 52-151-231). b) Oblique aerial photograph of the inner ring of Aorounga (view is from the north towards the south). Prominent light and dark streaks indicate wind erosion and sedimentation.

tend to dip towards the outside of the crater. The structure occurs in sandstones of probable Upper Devonian age (Wacrenier et al. 1958). Precambrian basement was not found exposed in the central uplift. Similar to Aorounga, no age information is known for this structure, aside from an upper limit derived from the possible Upper Devonian age of the target rocks.

REMOTE SENSING ANALYSIS

Shuttle Radar Topography Mission (SRTM) data (Farr and Kobrick 2000) were available for this study. Global SRTM single pass radar interferometry data (Farr and Kobrick 2000) were obtained from the NASA Jet Propulsion Laboratory. SRTM digital elevation model data have a horizontal resolution of 1 arc second (equivalent to 30 m at the equator) and a vertical resolution of 10 m, for the C-band radar. Global 3 arc second data have been released to date; 1 arc second data are only available for North America. Cowan and Cooper (2003a) made an initial comparison between 3 arc second SRTM and an older GTOPO DEM (Global Topography 30 arc second Digital Elevation Model) of the USGS and showed that the resolution of SRTM DEM is a significant improvement and will be particularly valuable in areas for which limited topographic data are available. For comparison with SRTM data, the Thematic Mapper (TM) Landsat 5 data (27 m resolution) for the Aorounga and Gweni Fada areas could be applied. Several enhancement methods, including fractional order sunshading (Cooper and Cowan 2003b, c) and a technique that enhances circular anomalies (Cooper 2003), were also utilized.

Aorounga

Figure 5a shows the Landsat 5 band 7-4-2 image for the Aorounga region. The area shown measures 54 and 52 km in E-W and N-S directions, respectively. The crater structure is well defined, with a broad, near-circular central area of an

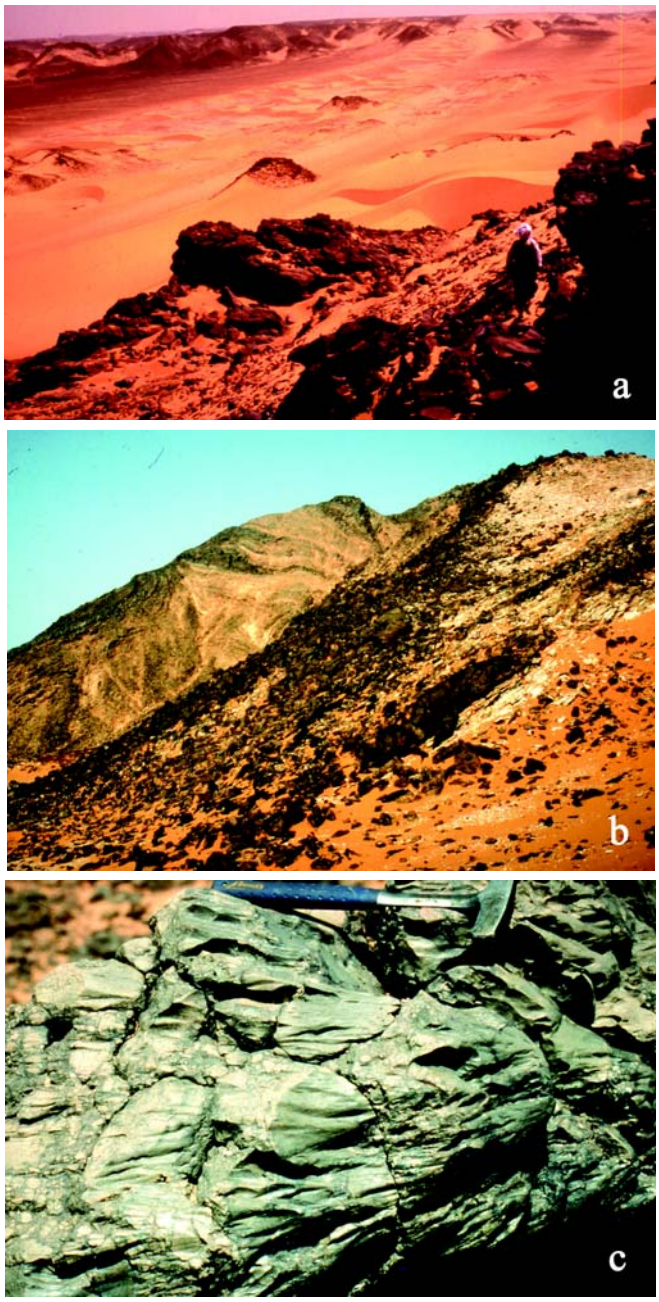

Fig. 3. Field photographs (by P. M. Vincent) of the Aorounga structure: a) a view from the inner ring (foreground) looking towards the north, across the middle depression; the outer ring is in the background. b) NW limit of outer depression; rock strata dip toward the interior depression. c) Fracturing phenomenon resembling shatter cones (40 cm long hammer, for scale).

obvious hilly terrain, of ~9 km in diameter. It is surrounded by a flat annulus (maximum 3 km wide), which shows at its outer edge disturbance from circular geometry, most likely through a series of faults that trend obliquely to the circumference of the structure. Especially in the western and southwestern sectors, a distinctly hummocky (mountainous) ring encloses the flat annulus. It is, however, difficult to identify how far out this ring structure extends, especially in the northeastern

Fig. 4. a) The Gweni Fada impact structure (space shuttle image STS 62-90-105). b) Oblique aerial photograph of the central uplift of the Gweni Fada structure, looking towards the southwest.

and southwestern sectors where the crater structure is surrounded by complex terrain. Regional trends are poorly defined, as the entire region is transgressed by an extensive system of NE-SW trending sandstone ridges and dunes. These ridges and, in the flatter parts, dunes also transgress across the crater structure and obscure much of the detail of the inner complex and the outer ring.

Figure 5b represents the SRTM raw topography data. The crater area is demonstrably complex in terms of topographic relief, and some more subdued topography is noted in the southwestern part of this image. This southwestern pattern resembles a drainage pattern. Similar patterns are also noted in some areas around the crater structure, and, in particular in the north, this could be interpreted as some fossil drainage off the crater rim. The longitudinal dunes are very subdued over much of this region, in particular in and around the crater structure. The crater interior shows a small, irregularly shaped central peak area surrounded by a somewhat flatter ring, in turn surrounded by a broad and topographically strong ring.

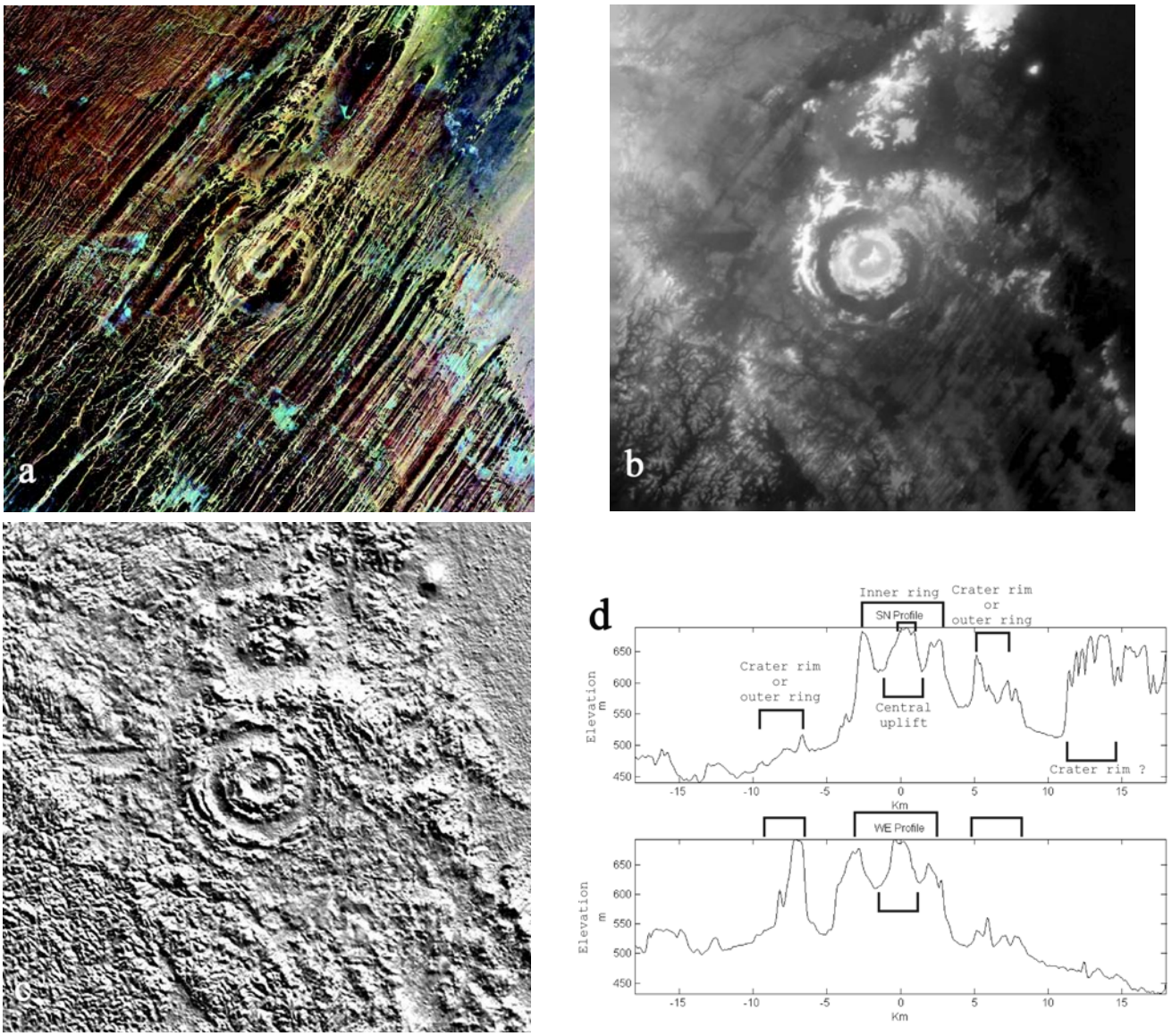

Fig. 5. Remote sensing analysis of Aorounga. a) Landsat 5, bands 7-4-2 image (resolution 27 m), with regional structure largely obscured by the impressive pattern of regional dunes. In this and the following images, north is up. b) Raw SRTM data providing a detailed representation of fossil-drainage at and in the environs (especially to the SW) of the Aorounga structure. c) Topography based on the SRTM data, with sunshading from the NE (which effectively removes the strong pattern of NE-SW trending longitudinal dunes). d) Two topographic profiles in N-S and E-W direction across the Aorounga impact structure (see text for detailed discussion).

A sunshaded (from the NE) image of the radar topography at and around Aorounga is shown in Fig. 5c. This enhancement results in a complete loss of the dune effect and provides a very detailed topographic impression. Aorounga impact structure is recognized as a multi-ring structure, which comprises a central, somewhat hummocky area, surrounded by a near-circular and 2 to 3 km wide ring feature of strong elevation, followed by the flat annulus and then by an outer ring, which is now recognizable as a feature that surrounds the entire crater structure—presumably the actual crater rim zone (compare Fig. 5d). In particular in the northeast and in the southwest, a series of ridges can be noted, and one is tempted to interpret this as a series of sedimentary strata.

Figure 5d illustrates two elevation profiles along the N-S and E-W lines across the crater structure and its environs. The profiles define significant relief of up to 230 m. A central complex of 7.5–8 km in width also contains a central peak of 2–2.5 km in diameter. The depression (a flat terrain around the central complex) is about 2 km wide and of even elevation in all four sectors of the crater structure. This feature is surrounded by a 3 to 3.5 km wide zone (outer ring) of variable but always significant relief. This ring feature probably represents the apparent crater rim of 16–17 km maximum diameter. Consequently, the previously accepted apparent crater diameter of 13 km may need to be revised.

Circular sunshading results (Fig. 5e) in an enhancement

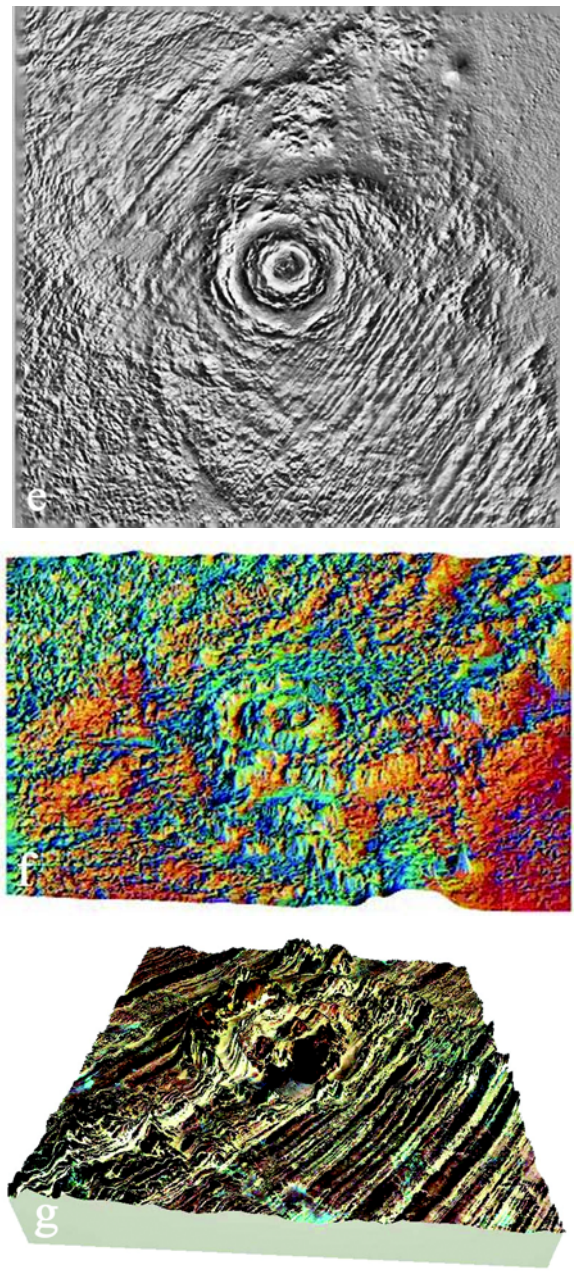

Fig. 5. *Continued.* Remote sensing analysis of Aorounga. e) Aorounga SRTM image after application of circular sunshading. This method confirms the maximum extent of this impact structure. f) Fractional order horizontal derivative sunshaded SRTM data overlain on the SRTM data (in 3-D). The sun inclination used was 30° from the horizontal, and the sun azimuth was in the northwest. g) A further 3-D perspective of the Aorounga crater structure produced by superposition of the Landsat image (compare to Fig. 5a) onto the SRTM topographic data.

of the NE-SW trending dune system, but depresses those in perpendicular orientation. The crater itself is enhanced, and it is now possible to speculate about the maximum outer diameter because, in the southwest, the ridges of the crater rim are clearly separated from the surrounding terrane. However, in the northeast, this is not achieved. If this had been caused by the pre-impact presence of a mountainous region that was (at least partially) impacted and thus structurally complicates the rim section to the northeast, then this would be analogous to the southern parts of the Bosumtwi impact crater. In the latter case, the crater is superposed onto the Obuom mountain range along the southern/southeastern margin of this structure (Wagner et al. 2002).

This effect is also noted in Fig. 5f, which shows the result of a calculation, in which gradients of 0.75, 1.00, and 1.25 were used in the reflectance algorithm. The resulting RGB color image was then superimposed onto a three-dimensional surface, the elevations of which were based on the original SRTM data. The result of this transformation is a detailed DEM image, where the various structural elements of the crater structure are much enhanced. This also enhances the small, though topographically well-defined, central peak in the centermost part of the structure. Seemingly, the ring structure surrounding this center is quite broad and could also be made of several upturned sedimentary strata, similar to the stratigraphy of the outer ring. The crater rim (outer ring) is well defined from south to northwest. Based on this image and the profiling of Fig. 5d, a maximum diameter for the Aorounga structure of 16 km is proposed. This image also illustrates that the drainage system visible in the raw radar data is related to the complex topography in the southwestern sector of the scene.

Finally, superposition of the Landsat 5 scene onto the SRTM data provides a realistic 3-D perspective of the crater region (Fig. 5g).

Gweni Fada

The nearly circular Gweni Fada structure stands out prominently in the Landsat 5 (band 7-4-2) image of Fig. 6a. It comprises an off-center (offset towards the south), apparently structurally complex, terrain that is surrounded in the western, northern, and eastern sectors by an apparently flattish terrain. Radial trends of both ridges and apparent drainage outward the elevated terrain surrounding the flat ring zone is quite obvious. However, there is also evidence of radially oriented drainage and sedimentation into the flat interior of the crater structure, which is especially noticeable in the western/northwestern sector. A well-defined drainage channel is visible in the eastern part of the flat zone, and the central complex terrain drains visibly towards the southeast. Strong drainage from the north and associated sedimentation into the crater is also indicated.

The SRTM raw data are shown in Fig. 6b. This image confirms the overall topographic impression obtained from the Landsat image, but in addition demonstrates the entirely different patterns of regional structure in the sectors to the north of the impact structure, within and around of the crater, and to the south/southwest. Apart from some drainage from the north and east, the immediate environs of the crater are dominated by quite featureless terrain. The sunshaded image

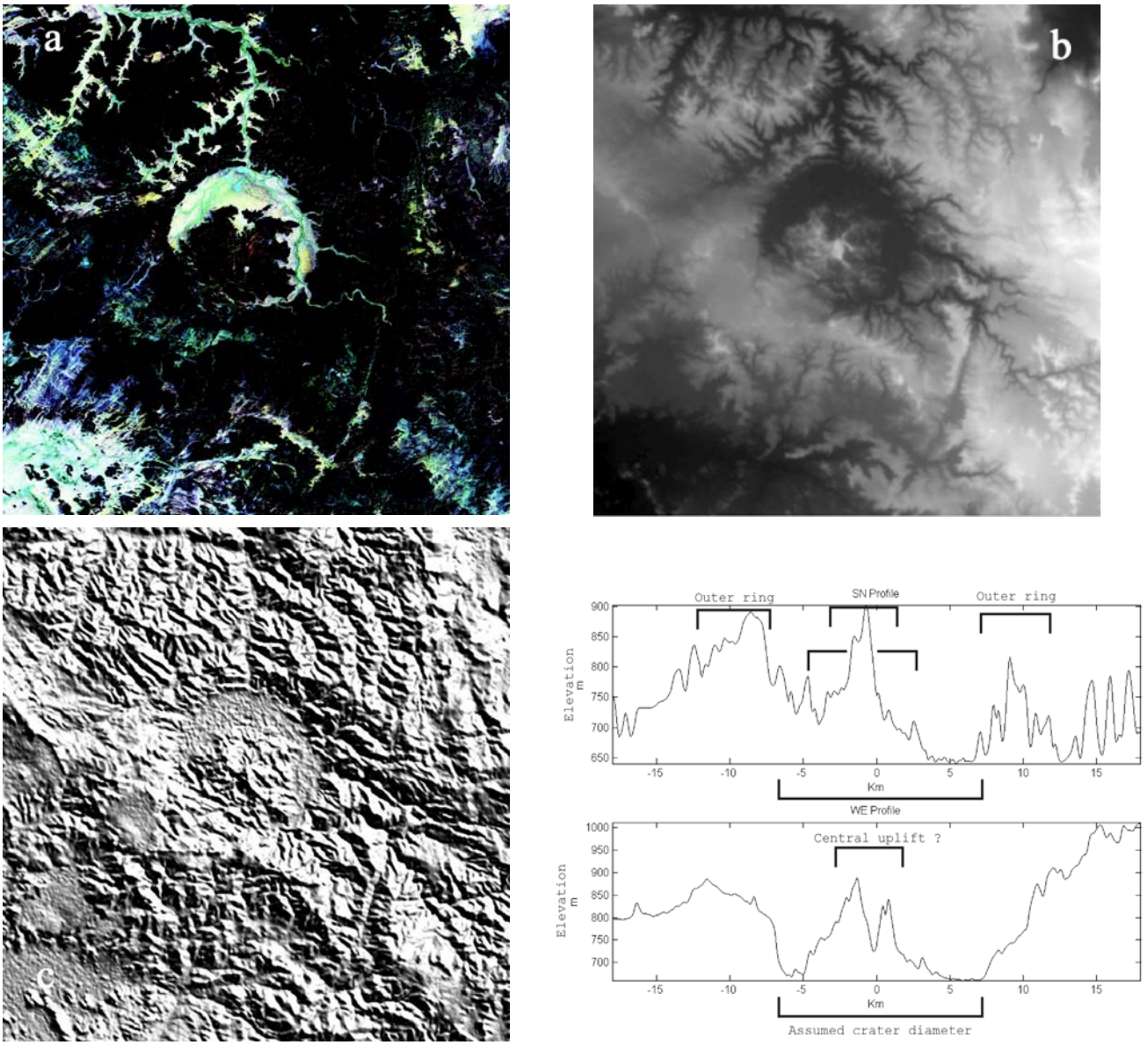

Fig. 6. Landsat and SRTM data and perspectives of the Gweni Fada impact structure. a) Landsat 5 bands 7-4-2 image. Note the limited topography indicated over the actual crater, but in contrast to the Aorounga case (Fig. 5a), detailed fossil and recent drainage is documented. b) SRTM raw data confirming much of the drainage pattern of Fig. 6a. c) This sunshaded (from the NE) topographic image based on the SRTM data indicates that the interior of the crater structure has complex terrain, which is not centered but offset towards the southern sector. d) Two elevation profiles across the Gweni Fada structure, in the N-S and E-W directions.

of Fig. 6c has a sun azimuth of 45 degrees E and an elevation of 30 degrees. Sunshading results in a considerable enhancement of the structural detail of the region. The central hilly terrain of the crater and the surrounding flat zone of very subdued topography are evident. Because of the complex structure of the crater environs, it remains difficult to define the crater rim zone. About 2 km into the environs, some vague indications of annular, radial, and tangential structure are noted. Two elevation profiles across the structure (Fig. 6d) illustrate that the maximum relief comprises 280 m. The close-to-circular shape of the structure is confirmed, but it is also noted that the topographically compressed zone is significantly narrower on the S and W sides than in the N and E. The broad central complex—presumably the collapsed central uplift—has a width of about 9 km, and complex geometry is also indicated in these profiles, as already noted. Maximum elevation in this terrain reaches 200 m above the ring basin. This “moat” is about 2–3 km wide. A broad outer ring comprising a series of ridges is best defined in the north. Because of the complex terrain of the surroundings of the crater, it is rather difficult to determine the width of this outer zone, and our best estimate is only some 4–5 km. If this estimate is correct, the actual apparent crater diameter would increase from the previous 12 km to 22–23 km. Based on the

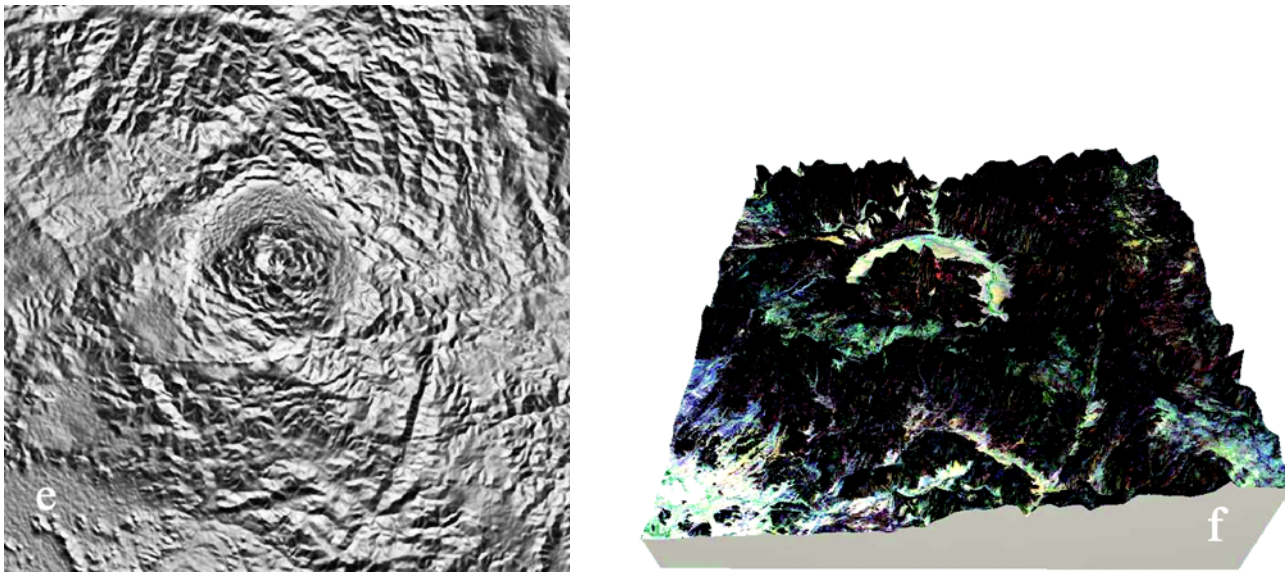

Fig. 6. *Continued.* Landsat and SRTM data and perspectives of the Gweni Fada impact structure. e) circular sunshading provides a definite placement and extent for this impact structure. Distinct NNE, NNW, and NW trends in the regional structure are also enhanced. f) Superposition of Landsat and SRTM data sets provides a realistic 3-D perspective, which particularly emphasizes the strong elevation in the south-central part of the crater structure.

relationship between apparent crater diameters and the corresponding central uplift diameters by Therriault et al. (1997; their Fig. 3), a structure of such diameter will have a likely central uplift diameter of 7–9 km, which is consistent with our observations for Gweni Fada.

An attempt to enhance geological structure in the Gweni Fada area by circular sunshading is shown in Fig. 6e. This clearly enhances the circularity of the actual crater structure, in contrast to the remaining area. In particular, there is a strong circular aspect to the northeastern to northwestern sector of the crater rim. Figure 6f was produced by superposition of the Landsat data onto the SRTM data. This three-dimensional perspective gives a strong impression of the presence of the outer ring, especially in the north where relief is highest in this zone, but also in the more subdued ring topography of the eastern and southern sectors surrounding the ring depression. Thus, we conclude that the likely diameter of the eroded Gweni Fada impact structure was about 21–23 km.

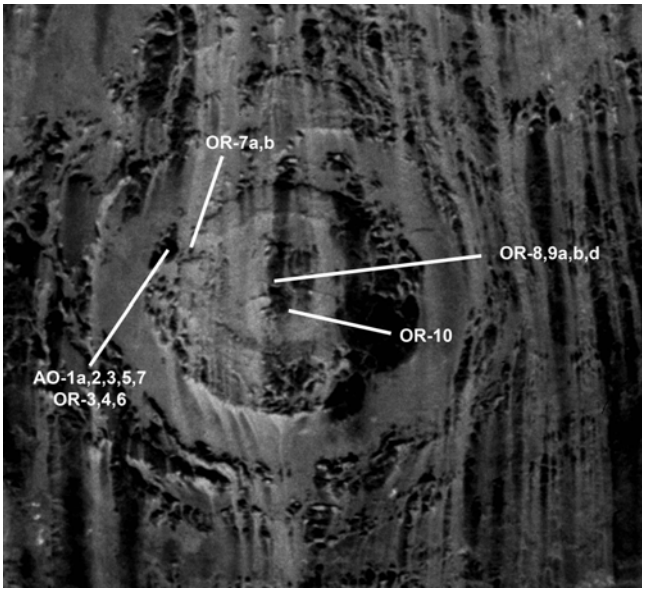

Fig. 7. A close-up of a shuttle image of Aorounga with locations of samples investigated in the present study.

PETROGRAPHY

Samples and Methods

Fifteen samples from the Aorounga impact structure and six samples from the Gweni Fada impact structure were collected by P. Vincent during a visit to the field area in the mid-1990s (cf. also Vincent and Beauvilain 1996). Sampling locations for the Aorounga samples (in the central parts of the structure) are shown in Fig. 7. The Gweni Fada samples all represent target rocks; GF-3 and GF-6 are quartzitic sandstones from the center of the structure; GF-8 is crushed/brecciated sandstone from the outer limit of the outer depression; GF-9 is crushed quartzite from the SW part of the central uplift; and GF-11 and GF-12 are quartzitic sandstones from the N part of the central uplift.

Thin sections of these samples were studied by optical microscopy to classify the rock type and to investigate any evidence of shock metamorphism. Crystallographic orientations of planar deformation features (PDFs) in quartz were measured on the optical microscope using a universal stage with four axes. Major element oxide and some trace

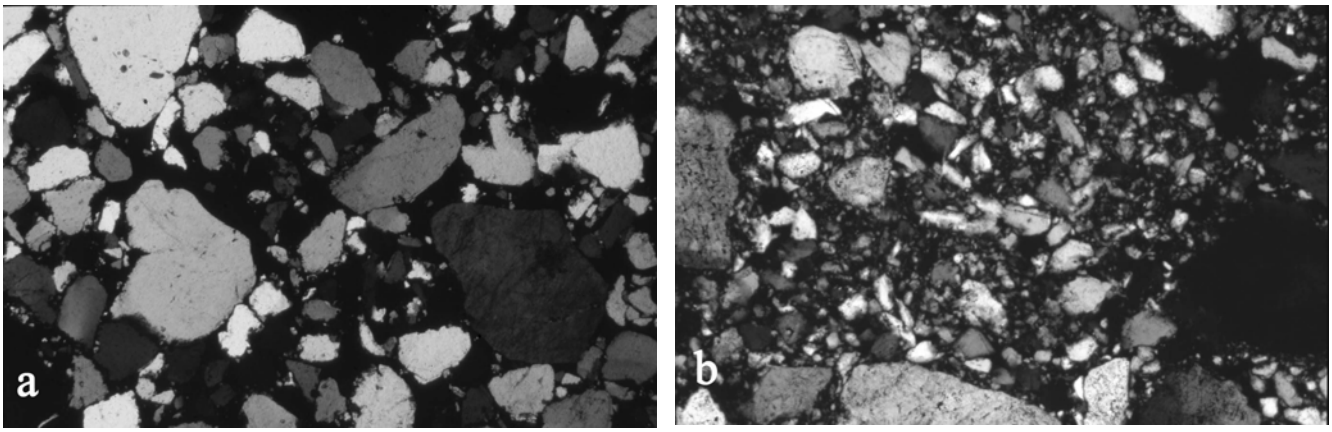

Fig. 8. Microphotographs of textures of typical target rocks. a) Sample AO-7; rounded to subrounded detrital quartz grains in quartzite, cemented with iron oxides; no apparent shock deformation (crossed polarizers, width of image 3.5 mm). b) Sample OR-3; patch of crushed quartz grains in finer-grained matrix (possibly some recrystallization after local melting), some alteration, remnants of PDFs in some of the grains (crossed polarizers, width of image 1.1 mm).

element concentrations were determined on powdered samples by X-ray fluorescence (XRF) spectrometry. Details on procedures, precision, and accuracy are similar to the account given by Reimold et al. (1994). Other trace elements, including the rare earth elements (REEs), were determined using instrumental neutron activation analysis (INAA). The quality of the data was monitored by the simultaneous analysis of international geological reference materials. Details of analytical procedures (instrumentation, standards, data reduction, accuracy, and precision) are given by Koeberl (1993). Rb-Sr and Sm-Nd isotopic compositions of some samples were determined by mass spectrometry according to the methods detailed by Reimold et al. (1999).

Results

Our samples from the Aorounga structure are derived from the top of the central part or the outer slope of the inner ring structure (see Fig. 7). In contrast to the appearance in the field, which led to the belief that some of these samples may represent impactites with fluidal textures, we conclude from our petrographic studies that all these samples represent quartzite or sandstone, some of which could represent monomict breccias. Lithologically, a number of rock types have been sampled, including pure orthoquartzite, less mature quartzites, and sandstones of variable grain size and grain shape, hematite-cemented sandstone, as well as arenites of variable degrees of recrystallization (two examples are shown in Figs. 8a, b). The cause of this recrystallization is not clear.

Most of our samples are shock-metamorphosed to variable degrees, ranging from slight fracturing to quartz with PDFs. Besides unshocked rocks, there is evidence of low (only displaying elastic deformation in the form of short microfractures in quartz), moderate (single sets of PDFs in only a few quartz grains per thin section), and high degrees of shock metamorphism (for details, see Table 1). In the latter case, a single sample (AO-2) shows at least one set of PDFs in every quartz grain, but many have up to five sets of PDFs of different crystallographic orientations. Two to three sets of PDFs are most abundant. However, this sample is exceptional in our suite and all other available Aorounga samples are characterized by significantly lower shock metamorphic degrees. Most of them only display planar fractures and no, or only rare, PDFs (compare Table 1). Examples of shock deformation in Aorounga samples (some planar fractures and abundant PDFs) are shown in Fig. 9. In a few barely deformed samples, no shock-characteristic deformation effects were found. However, at a number of grain boundaries short (less than 15–20 μm) fractures emanate, sometimes in a nice radial fashion, from the contact points between adjacent quartz crystals, which demonstrates compressional stress.

Unfortunately, only a very limited number of samples from Gweni Fada were available for our study. These samples also represent a suite of arenitic lithologies, including quartzite, hematite-stained sandstone, a pebbly sandstone, and a quartz conglomerate. These samples are derived from the central disturbed area, as well as from the outer margin of the ring depression. Some limited alteration is indicated by hematite staining and cementation. Some samples are apparently unshocked (i.e., no characteristic shock deformation relating to pressures in excess of 5 GPa were observed), but display minor deformation such as radial cracks emanating from points where adjacent quartz grains abut against each other. Other samples contain grains with single or multiple sets of PDFs, with two sets of PDFs per grain being the most common, at variable frequency. In addition, local brecciation in the form of micro-veins, or in some samples rather pervasive brecciation, was noted. It appears that the presence of such cataclastic zones is limited to samples that have very few or no PDFs. Thus, the

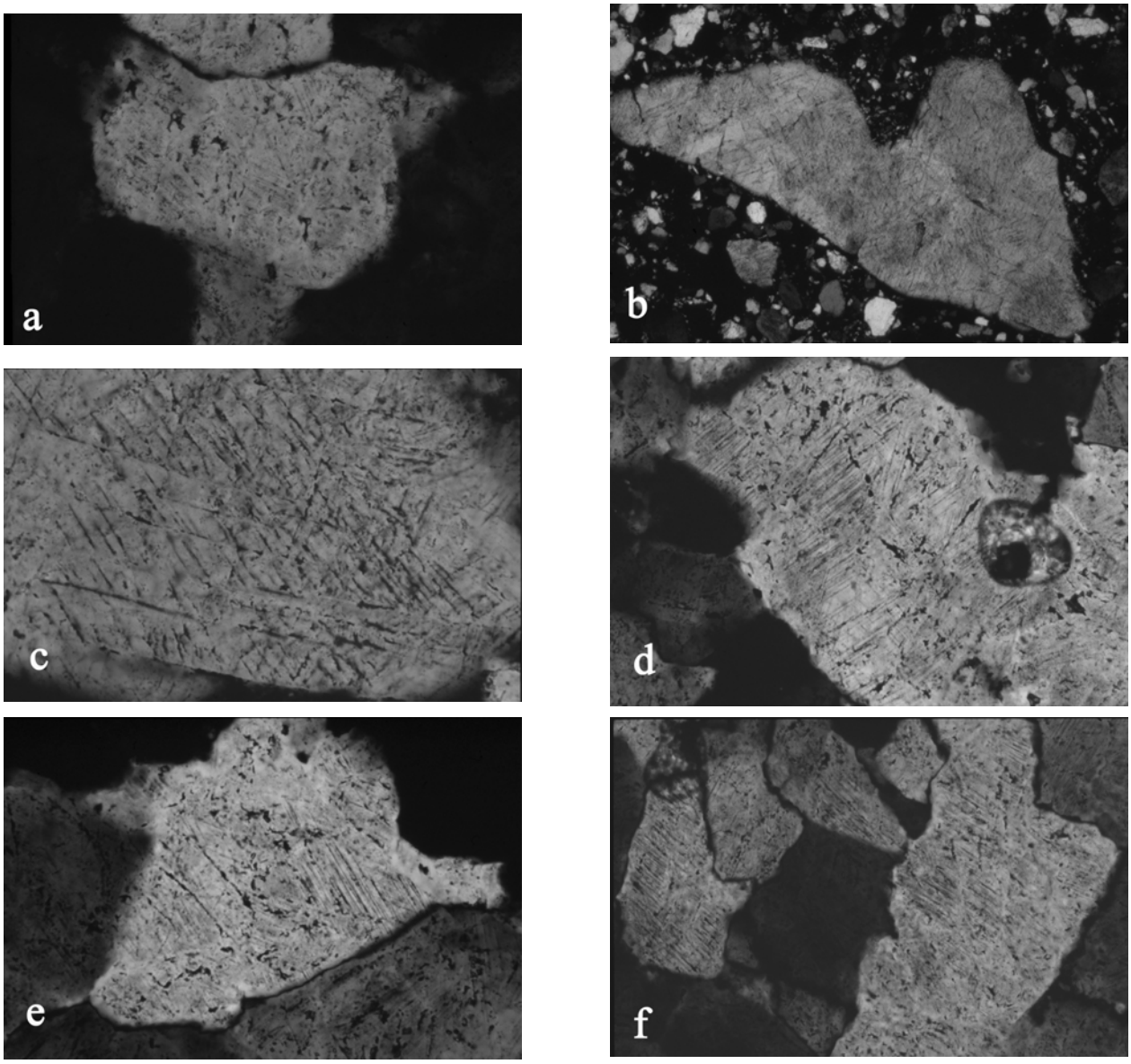

Fig. 9. Microphotographs of shock features in basement rocks and monomict breccias of the Aorounga impact structure (all photos taken with crossed polarizers). a) Sample AO-2; quartz grain in mature orthoquartzite, showing three sets of PDFs (image 355 µm wide). b) Sample OR-7a, monomict impact breccia; quartz grain with abundant planar fractures and PDFs (2 sets visible in image between fracture planes) (image 355 µm wide). c) Sample OR-9b; at least two, possibly three sets of PDFs between subplanar fractures in large quartz grain (image 355 µm wide). d) Sample AO-2; three sets of PDFs in large quartz grain (image 565 µm wide). e) Sample AO-2; two sets of well-defined PDFs in quartz grain, which also shows toasting (image 365 µm wide). f) Sample OR-4, several quartz grains with two to three sets of PDFs visible in photo; some planar fracturing is visible as well (image 1.1 mm wide).

deformation level for these samples is estimated at <15 GPa, in accordance with the limited manifestation of PDFs in samples experimentally shocked to this level (e.g., Huffman and Reimold 1996). From the limited number of samples available, we cannot reliably distinguish differences in the degree of shock versus sample location.

The results of the orientation measurements on 38 planes in 22 quartz grains from four samples from Aorounga show clearly that the shock-characteristic orientations (0001), $\{10\bar{1}3\}$, $\{10\bar{1}2\}$, $\{11\bar{2}2\}$, $\{10\bar{1}1\}$, and $\{21\bar{3}1\}$ are present (e.g., Stöffler and Langenhorst 1994; Grieve et al. 1996). A histogram showing the orientation of the poles of the PDF planes relative to the c-axis of the quartz grains is given in Fig. 11a. Only 16 planes in 10 grains from one sample of Gweni Fada were measured for their crystallographic orientations (Fig. 11b). With the exception of the $\{10\bar{1}2\}$ orientations that are missing in the Gweni Fada case, the two histograms are very similar. The histograms show the usual impact-characteristic orientations with a significant proportion of the higher angles. Similar orientation patterns

Table 1. Shock petrographic description of samples from Aorounga (AO, OR) and Gweni Fada (GF), including shock level estimates.

AO-1A: Very rare PDFs, but abundant grains with one set or multiple sets of PFs. Estimated shock level (based primarily on our past shock experimentation with Hospital Hill quartzite (Reimold and Hoerz [1986]; Huffman and Reimold [1996]): ~8–12 GPa.

AO-2: Strongly shocked sample: nearly every grain has at least one set of PDFs, many up to three, and numerous sets of PFs were observed, many of which are rather narrow-spaced (~20–25 GPa).

AO-3: No PDFs, only a few grains with one or two sets of widely spaced PFs (~5–8 GPa).

AO-5: A handful of grains with one set of PFs, one grain with two sets of PFs, and one grain with one set of PDFs (~8–10 GPa).

AO-7: No characteristic shock deformation. Unshocked sample. Only rare, irregular fractures and fluid inclusion trails, very little undulatory extinction.

OR-3: Similar to OR-4, but has a small number of grains with one set of PDFs and several grains with clearly reduced birefringence (~10–15 GPa).

OR-4: Numerous grains with undulatory extinction and up to two sets of PFs per grain. Many quartz crystals display the short and dense, often divergent shock extension fractures that we have previously described from a number of impact structures and that signify shock pressures <8 GPa. No PDFs (~6–8 GPa).

OR-6: Some undulatory extinction and a few grains with one set of generally widely spaced PFs (~5–8 GPa).

OR-7A: Some undulatory extinction in the form of waves or rare, subangular domains. A large number of grains with quite densely spaced and short extension fractures, as produced in 5 GPa shock experiments with quartzite. Considerable number of grains with one or two sets of PFs. A comparatively very large grain (~1 mm long) with three sets of densely spaced and well-developed PFs (~6–8 GPa).

OR-7B: Basically unshocked sample—only minor irregular fracturing. At maximum, ~1–3 GPa (?).

OR-8B: A large number of grains with 1–3 sets of PFs (three sets very rare), and a mere handful of grains with one set of short, decorated PDFs (~8–10 GPa).

OR-9A: Similar to OR-9B, but far fewer (actually only a few) grains with PFs and shock extension fracture arrays (~5 GPa).

OR-9B: Abundant grains with up to 3 sets of PFs; no PDFs noted. Grains often have dense and closely spaced arrays of short, generally slightly curved and often divergent extension fractures (~6–8 GPa).

OR-9D: Many grains with subplanar fractures, but only a few with well-developed, straight PFs. No PDFs observed. However, there are a few grains with two sets of PFs that are very densely spaced (~3–6 micrometers) (~8 GPa).

OR-10: Some grains with extensive, irregular fracturing, including several with single or multiple sets of short extension fractures. In addition, abundant grains with 1–3 sets of widely-spaced PFs, as well as a relatively small number of grains with single but very well-developed sets of more densely spaced PFs. Also, three grains with two sets of PDFs, all of which are rather large clasts entirely surrounded by fine-grained clastic groundmass (likely the specific setting is responsible for this local increase in shock deformation) (~8–12 GPa).

GF-3: Only irregular fracturing, never densely spaced, but sometimes enhanced at grain boundaries and grain contact points. No PFs or PDFs. If shock overprint present at all, <3 (?) GPa.

GF-6: Even less irregular fracturing than in GF-3: at most a few irregular fractures per grain. Sometimes enhanced at grain contacts (indicating strong compressional strain) Some (minor) undulatory extinction and deformation bands (<3 (?) GPa).

GF-8: Similar to GF-6, but even less deformation. Basically unshocked (<3 GPa).

GF-9: Entirely lacking deformation, besides very rare irregular fractures. No indication that this would be shock derived (<1 GPa).

GF-11: Lots of strongly fractured grains, with often well-developed single sets of subplanar fractures across entire crystals. Many relatively large grains with one or two sets of short PDFs (~15–20 GPa).

GF-12: Many grains with short shock extension fracture arrays and single sets of PFs. These hardly even cross entire grains. Rare grains with one set of PDFs, some of which are decorated. Like PFs, PDFs are generally short and only occur sporadically in selected areas of a crystal. Minor kinkbanding in the minor muscovite component of this sample. Planar and subplanar fracturing are enhanced along grain margins and local (point) contacts (~8–10 GPa).

General scaling of estimated shock pressures after, e.g., Stöffler and Langenhorst (1994); Huffman and Reimold (1996):

1–3 GPa: basically unshocked, only some irregular fracturing as result of shock overprint.

~5 GPa: onset of significant development of arrays of short shock extension fractures.

5–8 GPa: significant development of extension fracturing and planar fractures.

8 GPa: onset of PDF development, PFs prominent.

8–15 GPa: PFs prominent and 1–2 sets of PDFs significant.

15–20 GPa: two sets of PDFs prominent.

20–30 GPa: multiple sets of PDFs prominent and beginning isotropization at upper end of this range.

for shocked quartz of sedimentary rocks have been reported by others (e.g., Grieve and Therriault 1995; Grieve et al. 1996; French 1998), and it remains to be seen whether this is characteristic of shock deformation of sandstone and related sedimentary rocks. It is obvious from this work that sample textures play an important role regarding the development of shock features. In inequigranular samples, the relatively rare, larger particles seem to be consistently shock-deformed at higher levels than the smaller grain size fractions. Variable amounts of groundmass and degrees of clast packing also seem important.

GEOCHEMISTRY

The chemical compositions of the Aorounga and Gweni Fada samples are very similar (Tables 2 and 3), which is not a surprise given that both structures are thought to expose the same Upper Devonian stratigraphy. The major element compositions are silica-rich and correspond to typical sandstone compositions. With the exception of some samples that show hematite-staining, the SiO_2 contents range from about 88.4 to 97.7 wt%. The other major elements show a somewhat wider range in abundance, which is mainly due to

Table 2. Major and trace element composition of 15 samples from the Aorounga impact structure, Chad.

	AO-1a	AO-2	AO-3	AO-5	AO-7	OR-3	OR-4	OR-6	OR-7a	OR-7b	OR-8b	OR-9a	OR-9b	OR-9d	OR-10
SiO_2	94.32	96.95	97.19	98.68	88.46	95.75	95.85	94.65	88.44	81.73	96.11	90.41	95.36	96.85	97.66
TiO_2	0.19	0.26	0.07	0.07	0.12	0.16	0.10	0.14	0.62	0.44	0.09	0.22	0.09	0.17	0.11
Al_2O_3	3.03	1.46	1.42	0.27	0.61	1.42	2.22	0.51	6.87	4.96	2.20	3.57	1.99	0.90	1.22
Fe_2O_3	0.18	0.26	0.09	0.11	8.97	0.70	0.42	3.57	0.66	9.43	0.23	3.22	1.09	0.88	0.14
MnO	0.09	0.05	0.02	0.02	0.01	0.04	0.02	0.02	0.02	0.02	0.02	0.05	0.09	0.03	0.02
MgO	0.23	0.02	0.11	0.04	0.07	0.14	0.09	0.11	0.14	0.07	0.05	0.12	<0.02	0.03	0.02
CaO	0.23	0.11	0.04	0.09	0.03	0.49	0.05	0.09	0.09	0.09	0.05	0.19	0.04	0.16	0.05
P_2O_5	0.14	0.02	<0.02	<0.02	0.03	<0.02	0.02	0.02	0.03	0.07	0.02	0.14	0.04	0.05	0.04
L.O.I.	1.34	0.70	0.79	0.26	1.54	1.13	1.16	0.44	2.85	2.86	1.12	1.94	1.05	0.97	0.57
Total	99.75	99.83	99.73	99.54	99.89	99.83	99.93	99.55	99.72	99.67	99.89	99.86	99.75	100.04	99.83
Na	77	64	54	38	36	82	101	130	187	78	57	232	68	52	56
K	81	180	140	38	85	125	140	210	848	397	124	123	80	75	53
Sc	2.15	2.55	1.02	0.29	0.98	1.37	1.77	1.28	7.24	8.32	1.17	1.77	0.95	1.26	1.46
V	<20	<20	<20	<20	<20	<20	<20	<20	33	57	<20	29	<20	<20	<20
Cr	17.3	18.5	12.2	23.5	22.5	21.8	15.2	23.8	33.8	32.8	12.3	33.2	26.4	25.3	27.9
Co	1.02	0.74	0.34	0.17	1.81	0.39	0.23	7.98	1.87	15.5	0.29	0.73	0.76	0.41	0.22
Ni	11	6.2	3.9	2	20	8.8	5.8	21.3	23	38	7.2	2.7	10	5.4	11
Cu	21	24	7	10	6	10	9	57	30	49	8	15	25	31	15
Zn	11	5.1	3.3	3.1	17	4.7	3.2	20	88	319	2.5	7.2	4.5	4.9	2.5
Ga	2.4	2.1	0.9	0.3	1.9	1.5	0.9	4.2	14	7.9	0.9	1.4	5.2	0.7	2.5
As	3.02	5.31	0.41	0.69	2.48	2.37	2.11	17.5	2.96	14.2	0.73	4.84	1.61	2.21	0.67
Se	0.25	0.18	0.12	0.11	0.24	0.36	0.18	19.3	0.65	1.39	0.14	1.09	0.32	0.19	0.06
Br	0.31	0.27	0.32	0.26	0.35	0.39	0.39	0.28	0.38	0.58	0.37	0.71	0.29	0.38	0.42
Rb	0.68	1.14	0.27	0.22	1.61	0.79	1.11	2.31	4.49	2.25	0.51	1.12	0.98	0.54	1.38
Sr	45	15	23	4	11	23	47	23	36	20	28	39	55	46	30
Y	9	26	23	17	<8	9	10	25	21	33	13	<8	<8	27	24
Zr	199	268	111	79	128	155	134	200	426	350	122	202	91	175	146
Nb	9.0	7.0	8.0	<6	<6	6.0	12.0	9.0	14.0	10.0	11.0	9.0	<6	8.0	6.0
Sb	0.12	0.21	0.088	0.046	0.41	0.25	0.15	2.49	0.29	0.85	0.06	0.17	0.07	0.11	0.07
Cs	0.026	0.086	0.045	0.013	0.045	0.029	0.12	0.033	0.11	0.036	0.017	0.036	0.029	0.013	0.02
Ba	134	88	43	29	88	81	85	353	140	100	42	85	88	72	59
La	31.2	13.1	21.2	0.82	12.1	22.7	28.9	10.5	33.8	22.8	22.4	21.4	34.5	38.4	20.3
Ce	46.7	23.1	31.8	1.29	18.4	38.4	40.7	14.1	59.5	43.1	30.6	30.6	49.1	51.1	31.4
Nd	25.7	10.9	14.1	0.72	8.6	14.9	17.1	6.5	27.8	22.8	13.2	13.9	17.6	21.1	16.7
Sm	3.87	1.84	2.29	0.16	1.28	2.11	2.15	0.98	5.05	4.11	1.91	1.54	1.81	2.48	2.89
Eu	0.63	0.31	0.44	0.024	0.28	0.33	0.37	0.31	0.85	0.68	0.38	0.28	0.34	0.45	0.55
Gd	2.17	1.24	1.73	0.18	1.31	1.85	2.09	0.65	4.58	2.91	1.49	1.31	1.67	1.75	2.27
Tb	0.35	0.24	0.18	0.033	0.23	0.19	0.23	0.15	0.64	0.53	0.25	0.23	0.17	0.23	0.22
Tm	0.14	0.15	0.076	0.025	0.092	0.094	0.1	0.1	0.33	0.24	0.081	0.12	0.071	0.11	0.079
Yb	0.91	0.93	0.46	0.17	0.54	0.47	0.51	0.75	2.48	1.79	0.57	0.85	0.43	0.54	0.51
Lu	0.14	0.14	0.058	0.026	0.084	0.069	0.081	0.11	0.34	0.25	0.071	0.11	0.056	0.075	0.071
Hf	5.39	7.31	2.96	2.15	3.67	4.11	3.55	5.86	11.8	8.98	3.21	5.91	2.34	4.65	3.76
Ta	0.31	0.36	0.14	0.034	0.23	0.19	0.16	0.27	0.93	0.59	0.15	0.37	0.17	0.23	0.17
W	0.62	0.93	0.22	0.084	0.11	0.76	0.56	0.13	2.27	1.85	0.32	0.46	0.32	0.57	0.19
Ir (ppb)	<0.4	<0.5	<0.1	<0.05	0.05	0.06	<0.2	<0.2	<0.3	<0.4	<0.1	0.11	0.05	<0.2	<0.1
Au (ppb)	0.4	0.4	0.6	0.1	0.4	0.1	0.1	0.5	0.5	0.4	0.1	0.4	0.3	0.1	0.4

Table 2. *Continued.* Major and trace element composition of 15 samples from the Aorounga impact structure, Chad.

	AO-1a	AO-2	AO-3	AO-5	AO-7	OR-3	OR-4	OR-6	OR-7a	OR-7b	OR-8b	OR-9a	OR-9b	OR-9d	OR-10
Th	4.32	3.17	3.75	0.32	3.43	4.89	4.48	1.68	11.7	9.33	3.44	4.35	3.27	5.42	3.75
U	1.11	0.87	0.36	0.25	0.63	0.72	0.56	0.91	3.19	4.31	0.34	0.75	0.31	0.51	0.49
K/U	73	207	389	152	135	174	250	231	266	92	365	164	258	147	108
Zr/Hf	36.9	36.7	37.5	36.7	34.9	37.7	37.7	34.1	36.1	39.0	38.0	34.2	38.9	37.6	38.8
La/Th	7.22	4.13	5.65	2.56	3.53	4.64	6.45	6.25	2.89	2.44	6.51	4.92	10.55	7.08	5.41
Hf/Ta	17.4	20.3	21.1	63.2	16.0	21.6	22.2	21.7	12.7	15.2	21.4	16.0	13.8	20.2	22.1
Th/U	3.89	3.64	10.4	1.28	5.44	6.79	8.00	1.85	3.67	2.16	10.1	5.80	10.5	10.6	7.65
La_N/Yb_N	23.2	9.52	31.1	3.26	15.14	32.6	38.3	9.46	9.21	8.61	26.6	17.0	54.2	48.1	26.9
Eu/Eu*	0.66	0.63	0.68	0.43	0.66	0.51	0.53	1.19	0.54	0.60	0.69	0.60	0.60	0.66	0.66

Note: all major elements in wt%, trace elements in ppm (except as noted), all Fe as Fe_2O_3.

Table 3. Major and trace element composition of six samples from the Gweni Fada impact structure, Chad.

	GF-3	GF-6	GF-8	GF-9	GF-11	GF-12
SiO_2	89.85	93.76	97.71	92.24	95.38	92.31
TiO_2	0.19	0.13	0.09	0.45	0.14	0.58
Al_2O_3	3.00	1.25	1.04	2.86	2.31	4.49
Fe_2O_3	4.96	3.30	0.21	2.20	0.69	0.19
MnO	0.19	<0.02	0.03	0.07	0.02	0.02
MgO	0.07	<0.02	0.07	0.04	0.07	0.04
CaO	0.12	0.04	0.07	0.09	0.04	0.07
P_2O_5	0.02	0.06	0.03	0.07	<0.02	0.02
L.O.I.	1.59	0.90	0.73	1.60	1.05	1.85
Total	99.99	99.44	99.98	99.62	99.70	99.57
Na	29	31	35	41	20	82
K	60	79	115	210	570	1120
Sc	1.82	0.77	0.5	2.2	0.77	3.61
V	<20	<20	<20	230	<20	<20
Cr	14.1	18.9	13	65	13.2	24.5
Co	0.95	2.93	0.7	1.8	0.88	0.38
Ni	5.6	13	2.5	2.5	4.8	11
Cu	11	40	10	139	<3	<3
Zn	2.8	14	3.8	24	4.2	3.8
Ga	11	2.5	0.8	2.3	1.5	2.8
As	0.25	0.55	0.49	2.36	0.81	0.79
Se	0.05	0.19	0.05	0.16	0.07	0.07
Br	0.35	0.34	0.37	0.44	0.35	0.39
Rb	0.85	0.39	0.96	2.85	0.86	3.59
Sr	8	8	3	9	3	10
Y	<8	22	23	44	24	24
Zr	152	116	128	460	82	530
Nb	6.0	<6	7	15	10	17
Sb	0.03	0.03	0.04	0.11	0.07	0.12
Cs	0.01	0.025	0.022	0.010	0.051	0.11
Ba	28	10	39	82	11	57
La	5.35	9.87	5.68	22.1	8.41	27.4
Ce	9.69	21.2	9.46	36.9	13.6	50.9
Nd	4.9	9.7	4.9	17.8	6.2	23.3
Sm	0.69	1.53	0.76	3.25	1.05	3.52
Eu	0.065	0.25	0.11	0.51	0.21	0.54
Gd	0.63	1.61	0.63	3.21	0.82	3.35
Tb	0.083	0.15	0.089	0.38	0.11	0.43
Tm	0.078	0.071	0.065	0.21	0.062	0.24
Yb	0.52	0.51	0.44	1.33	0.39	1.79
Lu	0.089	0.078	0.054	0.21	0.053	0.28
Hf	4.12	3.23	3.51	13.3	2.21	14.7
Ta	0.25	0.19	0.11	0.52	0.11	0.75
W	0.47	0.16	0.19	0.85	0.16	1.08
Ir (ppb)	<0.2	<0.3	<0.2	<0.5	<0.2	<0.3
Au (ppb)	0.2	0.3	0.1	0.6	0.2	0.2
Th	3.47	3.49	2.17	9.31	1.46	10.4
U	1.12	0.66	0.53	1.99	0.54	2.57
K/U	54	120	217	106	1056	436
Zr/Hf	36.9	35.9	36.5	34.6	37.1	36.1
La/Th	1.54	2.83	2.62	2.37	5.76	2.63
Hf/Ta	16.5	17.0	31.9	25.6	20.1	19.6
Th/U	3.10	5.29	4.09	4.68	2.70	4.05
La_N/Yb_N	6.95	13.1	8.64	11.2	14.6	10.3
Eu/Eu*	0.30	0.49	0.49	0.48	0.69	0.48

Note: all major elements in wt%, trace elements in ppm (except as noted), all Fe as Fe_2O_3.

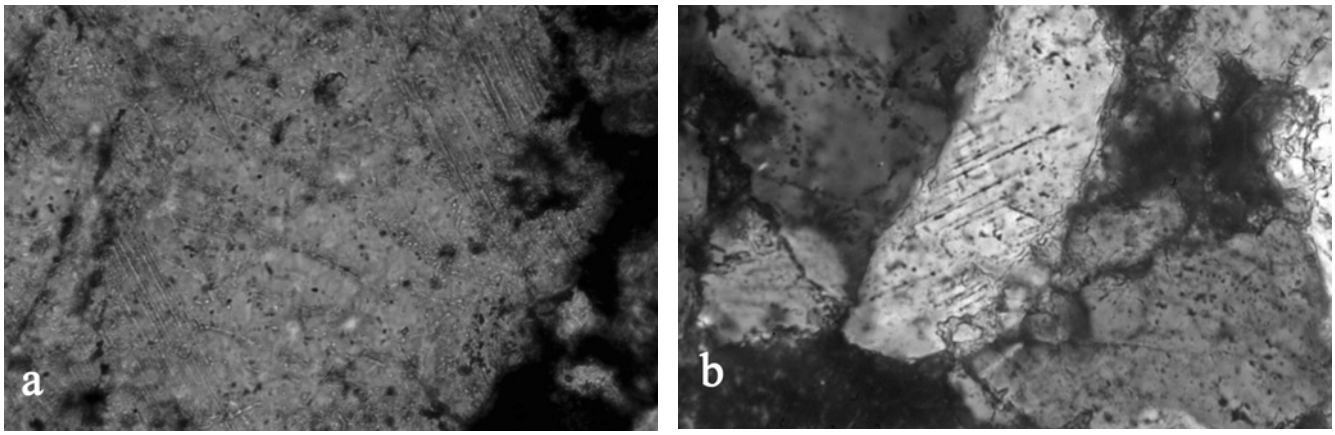

Fig. 10. Microphotographs of shock features in sample GF-12 (fine-grained quartzite) from the Gweni Fada impact structure: a) large quartz grain with up to three different orientations of PDFs (crossed polarizers; width of image: 2.3 mm); b) a close-up of a small quartz grain with one set of decorated PDFs; crossed polarizers, width of image 250 µm.

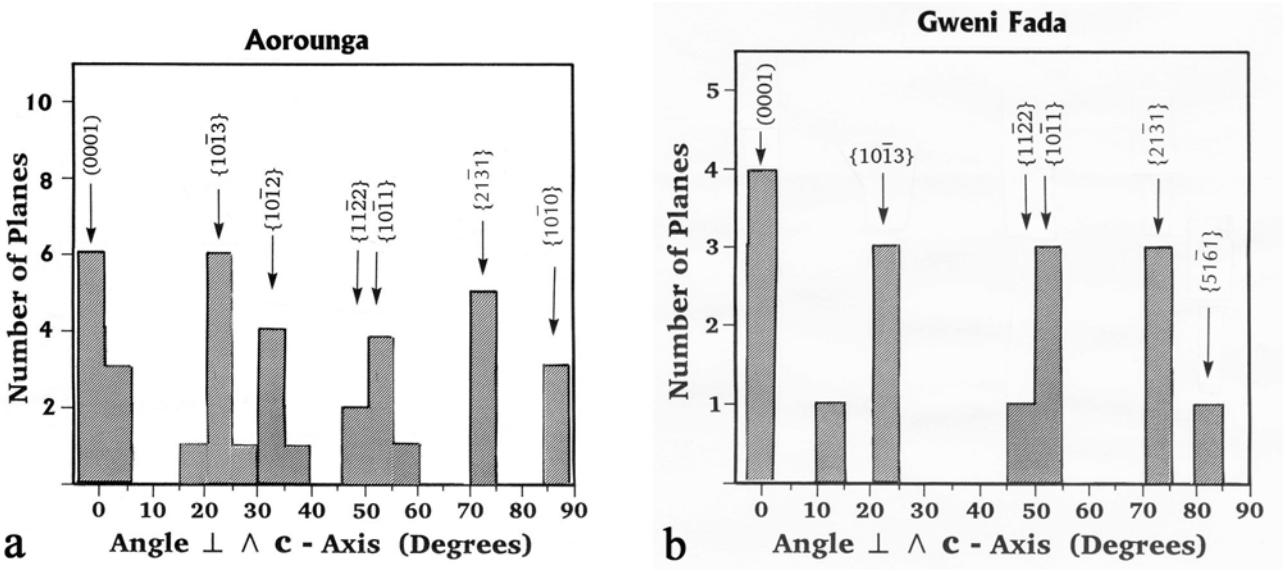

Fig. 11. a) Crystallographic orientations of PDFs in quartz from samples AO-2, OR-3, OR-7a, and OR-9d, from the Aorounga structure; 38 planes in 22 grains; b) crystallographic orientations of PDFs in quartz from sample GF-11 from the Gweni Fada structure; 16 planes in 10 grains.

the degree of hematite-staining and the presence of alteration products, including some carbonate. The overall limited chemical variation is reflected also by the trace element compositions, which are typical of crustal rocks (e.g., Taylor and McLennan 1985). The chondrite-normalized rare earth element patterns are also typical for upper crustal rocks, with La_N/Yb_N ratios of about 10 and minor to moderate negative Eu anomalies. Rb-Sr and Sm-Nd isotopic compositions were measured for three Aorounga and two Gweni Fada samples. The results for ε_{Sr} for AO-2, OR-7a, and OR-8b are +182.2, 222.0, and 201.7, and for GF-6 and GF-8 are +176.7 and +121.7; ε_{Nd} data for AO-2, OR-7a, and OR-8b are –7.6, –6.6, and –13.9, and the value for GF-8 is –6.4 (GF-6 was not measured). These values agree with upper crustal compositions (Taylor and McLennan 1985). No obvious siderophile element anomalies have been observed in any of the samples. Due to the quartz-rich nature of the samples, long counting times allowed to reach detection limits for Ir of 0.1 to 0.05 ppb. Only one sample (OR-9a) from Aorounga (a highly shocked rock, possibly a breccia) shows an Ir concentration of about 0.1 ppb, which is barely above the detection limit, but with a Ni value of only about 3 ppm, among the lowest of the range displayed by our samples.

CONCLUSIONS

We evaluated Shuttle Radar Topography Mission data for the Aorounga and Gweni Fada impact structures. We observed both radial structural complexity and topographic detail. Aorounga comprises an 9 km wide, structurally

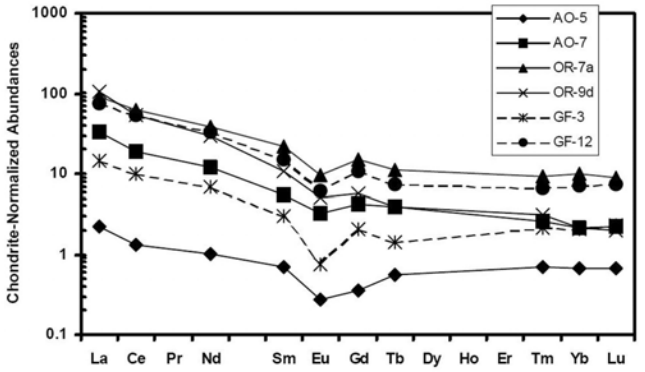

Fig. 12. Chondrite-normalized rare earth element abundances in three samples of the Aorounga and two samples of the Gweni Fada impact structure, Chad, showing the range of REE abundances encountered in the samples from both structures. The patterns are typical of upper crustal sedimentary rocks. Normalization factors from Taylor and McLennan (1985).

complex central zone, which is surrounded successively by a 2–3 km wide ring feature of low topography and an outer ring of about 3.5 km width, which could represent the crater rim. It appears that the previously accepted diameter for the Aorounga impact structure ought to be revised to about 16 km.

For Gweni Fada, the SRTM data allow us to distinguish a central, structurally complex and hilly terrain of about 9 km in diameter, which is surrounded by a much flatter terrane of 2–3 km in diameter. A broad, ~5 km wide, complex, zone forms the outer ring. Despite the difficulty to define the actual crater rim zone, a diameter of 22–23 km is now indicated for the Gweni Fada impact structure, which is significantly larger than the original estimated diameter of 14 km. The revised, larger diameter is, however, in good agreement with the scaling relationship (diameter versus central uplift diameter) for terrestrial impact structures proposed by Therriault et al. (1997).

Fifteen samples from the Aorounga and six samples from the Gweni Fada impact structures were studied to determine their petrographic and chemical characteristics. All samples represent target rocks, some of which have been brecciated (monomict breccia). Most of our samples show evidence of shock metamorphism in the form of PFs as well as PDFs in quartz grains. We found up to five PDF orientations per grain in one sample from Aorounga. Most other samples are characterized by ample development of PFs and a limited development of PDFs. For these reasons, at this stage, crystallographic orientations of PDFs cannot be evaluated spatially until further samples will become available. Orientation measurements on PDFs do show a predominance of the higher angles of the shock-characteristic orientations, which is in agreement with observations from shocked sedimentary rocks from other impact structures. The PDF statistics indicate maximum shock pressures of 20–25 GPa, based on abundance of multiple sets of PDFs, but mostly less than 10–15 GPa, based on the prominence of PFs and the occurrence of relatively rare, single sets of PDFs. These data quantify earlier indications of the occurrence of shock features (Becq-Giraudon et al. 1992; Vincent and Beauvilain 1996) and confirm the impact origin of both structures.

It is obvious that more thorough sampling of both impact structures is required to allow an in-depth study of shock degree versus PF and PDF development and their spatial distribution. This work would be very important in the light of the overall scarcity of shock deformation studies on sedimentary lithologies.

The chemical and isotopic compositions of all analyzed samples are typical for upper crustal silica-rich sedimentary rocks. No melt rocks or clasts, which might have been used in radiometric dating, were found in any of our samples. Both structures are well exposed in the field and should become subject of detailed ground-based investigations.

Acknowledgments–This work was supported by the Austrian Science Foundation FWF, project P17194-N10 (to C. K.) and the South African FRD (to W. U. R.). We are grateful to H. C. C. Cloete (Council for Geoscience, Pretoria) for the XRF analyses, and we acknowledge the Director, Council for Geoscience, for permission to perform the analyses. We are also grateful to F. J. Kruger and D. Brandt (both formerly of the University of the Witwatersrand) for help with the isotope analyses and U-stage measurements, respectively. D. Jalufka (University of Vienna) helped with graphics. Reviews by J. Spray and an anonymous reviewer, as well as editorial comments by U. Riller, are appreciated. This is University of the Witwatersrand Impact Cratering Research Group Contribution No. 87.

Editorial Handling—Dr. Ulrich Riller

REFERENCES

Becq-Giraudon J. F., Rouzeau O., Goachet E. and Solages S. 1992. Impact hypervéloce d'une météorite géante à l'origine de la dépression circulaire d'Aorounga au Tchad (Afrique). *Comptes Rendus Academie Science Paris* 315 (II):83–88.

Bourles D. L., Brown E.T., Raisbeck G. M., Yiou F., and Vincent P. 1995. Exposure age dating of the Aorounga (Sahara) impact crater by in-situ-produced ^{10}Be and ^{26}Al (abstract). EUG-8 Conference, Strasbourg, April 9–13, 1995.

Brandt D., Holmes H., Reimold W. U., Paya B. K., Koeberl C., and Hancox P. J. 2002. Kgagodi Basin: The first impact structure recognized in Botswana. *Meteoritics & Planetary Science* 37: 1765–1779.

Cooper G. R. J. 2003. Feature detection using sunshading. *Computers & Geosciences* 29:941–948.

Cowan D. R., and Cooper G. R. J. 2003a. The Shuttle Radar Topography Mission: A new source of near-global digital elevation data. *ASEG Preview* 107:27–29.

Cooper G. R. J. and Cowan D. R. 2003b. The application of fractional calculus to potential field data. *Exploration Geophysics* 34:51–56.

Cooper G. R. J. and Cowan D. R. 2003c. Sunshading geophysical

data using fractional order horizontal gradients. *The Leading Edge* 22:204–205.

Farr T. G. and Kobrick M. 2000. Shuttle Radar Topography Mission produces a wealth of data. *EOS Transactions* 81:583 and 585.

French B. M. 1998. *Traces of catastrophe: A handbook of shock-metamorphic effects in terrestrial meteorite impact structures.* LPI Contribution #954. Houston, Texas: Lunar and Planetary Institute. 120 p.

Grieve R. A. F. and Therriault A. M. 1995. Planar deformation features in quartz: Target effects (abstract). 26th Lunar and Planetary Science Conference. pp. 515–516.

Grieve R. A. F., Wood C. A., Garvin J. B., McLaughlin G,. and McHone J. F. 1988. Astronaut's guide to terrestrial impact craters. LPI Technical Report #88-03. Houston, Texas: Lunar and Planetary Institute. 89 p.

Grieve R. A. F., Langenhorst F., and Stöffler D. 1996. Shock metamorphism of quartz in nature and experiment: II. Significance in geoscience. *Meteoritics & Planetary Science* 31: 6–35.

Huffman A. R. and Reimold W. U. 1996. Experimental constraints on shock-induced microstructures in naturally deformed silicates. *Tectonophysics* 256:165–217.

Koeberl C. 1993. Instrumental neutron activation analysis of geochemical and cosmochemical samples: A fast and proven method for small sample analysis. *Journal of Radioanalytical and Nuclear Chemistry* 168:47–60.

Koeberl C. 1994. African meteorite impact craters: Characteristics and geological importance. *Journal of African Earth Sciences* 18: 263–295.

Koeberl C. and Reimold W. U. 2003. Geochemistry and petrography of impact breccias and target rocks from the 145 Ma Morokweng impact structure, South Africa. *Geochimica et Cosmochimica Acta* 67:1837–1862.

Koeberl C., Armstrong R. A., and Reimold W. U. 1997. Morokweng, South Africa: A large impact structure of Jurassic-Cretaceous boundary age. *Geology* 25:731–734.

Koeberl C., Reimold W. U., Vincent P. M., and Brandt D. 1998. Aorounga and Gweni Fada impact structures, Chad, Central Africa: Petrology and geochemistry of target rocks (abstract #1103). 29th Lunar and Planetary Science Conference. CD-ROM.

Master S. and Reimold W. U. 2000. The impact cratering record of Africa: An updated inventory of proven, probable, possible, and discredited impact structures on the African continent. In *Catastrophic events and mass extinctions: Impacts and beyond.* LPI Contribution #1053. Houston, Texas: Lunar and Planetary Institute. pp. 131–132.

Miallier D., Sanzelle S., Falguères C., Faïn J., Pilleyre T., and Vincent P. M. 1997. TL and ESR of quartz from the astrobleme of Aorounga (Sahara of Chad). *Quaternary Science Reviews* 16: 265–274.

Miller R. McG. and Reimold W. U. 1986. Deformation and shock deformation in rocks from the Roter Kamm crater, SWA/ Namibia. *Meteoritics* 21:456–458.

Reimold W. U. and Hoerz F. 1986. Experimental shock metamorphism of Witwatersrand quartzite (abstract). Geocongress'86, Biennial Congress of the Geological Society of South Africa. pp. 53–57.

Reimold W. U., Koeberl C., and Bishop J. 1994. Roter Kamm impact crater, Namibia: Geochemistry of basement rocks and breccias. *Geochimica et Cosmochimica Acta* 58:2689–2710.

Reimold W. U., Koeberl C., Brandstätter F., Kruger F. J., Armstrong R. A., and Bootsman C. 1999. The Morokweng impact structure, South Africa: Geological, petrological, and isotopic results, and implications for the size of the structure. Proceedings, Conference on Large Meteorite Impacts and Planetary Evolution. GSA Special Paper #339. Boulder, Colorado: Geological Society of America. pp. 61–90.

Roland N. W. 1976. Die Ringstruktur Aorounga (Borkou, Süd-Sahara). *Geologisches Jahrbuch* 33:117–131.

Stöffler D. and Langenhorst F. 1994. Shock metamorphism of quartz in nature and experiment: I. Basic observations and theory. *Meteoritics* 29:155–181.

Taylor S. R. and McLennan S. M. 1985. *The continental crust: Its composition and evolution.* Oxford: Blackwell Scientific Publications. 312 p.

Therriault A. M., Grieve R. A. F., and Reimold W. U. 1997. Original size of the Vredefort structure: Implications for the geological evolution of the Witwatersrand Basin. *Meteoritics & Planetary Science* 32:71–77.

Vincent P. M. and Beauvilain A. 1996. Découverte d'un nouveau cratère d'impact météoritique en Afrique: l'astroblème de Gweni Fada (Ennedi, Sahara du Tchad). *Comptes Rendus de l'Academie des Sciences* 323 (II):987–997.

Wacrenier P., Hudeley H., and Vincent P. M. 1958. Carte géologique du Borkou-Ennedi-Tibesti à 1/100,000. Brazzaville: Direction des Mines et la Géologie.